

Catching Time-Reversed Microwave Coherent State Photons with 99.4% Absorption Efficiency

J. Wenner,¹ Yi Yin,^{1,2} Yu Chen,¹ R. Barends,¹ B. Chiaro,¹ E. Jeffrey,¹ J. Kelly,¹ A. Megrant,^{1,3} J. Y. Mutus,¹ C. Neill,¹ P. J. J. O'Malley,¹ P. Roushan,¹ D. Sank,¹ A. Vainsencher,¹ T. C. White,¹ Alexander N. Korotkov,⁴ A. N. Cleland,¹ and John M. Martinis^{1,*}

¹*Department of Physics, University of California, Santa Barbara, California 93106, USA*

²*Department of Physics, Zhejiang University, Hangzhou 310027, China*

³*Department of Materials, University of California, Santa Barbara, California 93106, USA*

⁴*Department of Electrical Engineering, University of California, Riverside, California 92521, USA*

(Received 15 November 2013; revised manuscript received 24 January 2014; published 28 May 2014)

We demonstrate a high-efficiency deterministic quantum receiver to convert flying qubits to stationary qubits. We employ a superconducting resonator, which is driven with a shaped pulse through an adjustable coupler. For the ideal “time-reversed” shape, we measure absorption and receiver fidelities at the single microwave photon level of, respectively, 99.41% and 97.4%. These fidelities are comparable with gates and measurement and exceed the deterministic quantum communication and computation fault-tolerant thresholds, enabling new designs of deterministic qubit interconnects and hybrid quantum computers.

DOI: [10.1103/PhysRevLett.112.210501](https://doi.org/10.1103/PhysRevLett.112.210501)

PACS numbers: 03.67.Lx, 42.50.Ct, 42.50.Ex, 85.25.Cp

Systems coupling qubits and cavities provide a natural interface between fixed logic qubits and flying photons. They have enabled a wide variety of important advances in circuit quantum optics, such as generating novel photon states [1–3] and developing a toolbox of quantum devices [4–7]. Hybrid quantum devices and computers [8,9] can be implemented between superconducting coplanar waveguides and micromechanical oscillators or superconducting, spin, and atomic qubits [10–14]. For such implementations, it can be advantageous to employ deterministic quantum state transfer [15,16], which needs highly efficient quantum transmitters and receivers.

For deterministic quantum networks [17], it is particularly challenging to convert flying qubits to stationary qubits, since absorbing naturally shaped emission has a maximum fidelity of only 54% [18,19]. Theoretical protocols reaching 100% efficiency rely upon sculpting the time dependence of photon wave packets and receiver coupling [20–22]. To accomplish this, recent experiments have developed transmitters with adjustable coupling [23–25]. However, experimental reception fidelities have reached a maximum of only 88% for optical photons [26] and 81% for microwave photons [14]. These are well below fidelities required for fault-tolerant deterministic quantum communication (96% [27]) and computation (99.4% [28]). Hence, only heralded schemes [29–31] were plausible to transfer quantum information between even adjacent quantum processors.

We demonstrate here a quantum receiver that absorbs and stores photons with a fidelity above the threshold fidelities for fault tolerance. We classically drive a superconducting coplanar waveguide resonator through an adjustable coupler, which we use as an on-off switch, with

a particularly simple “time-reversed” photon shape. At the single microwave photon level, we measure an absorption efficiency of 99.4% and a receiver efficiency of 97.4%. As these efficiencies are comparable to fidelities of good logic gates and measurements [32–36] and are for the first time above the threshold for fault-tolerant deterministic quantum communication, deterministic interconnects are possible between devices on nearby but separate chips.

The protocol we implement relies on time-reversal symmetry [20,37] between resonator energy absorption and emission. A resonator emits a photon wave packet which naturally decays exponentially in amplitude, as shown in Fig. 1(a). By time-reversal symmetry, the resonator will thus absorb an exponentially increasing wave packet with perfect efficiency [18,19,38].

More physically, the resonator perfectly absorbs a traveling wave packet if destructive interference occurs between signals reflected off the coupler and re-emitted (leaked) out of the resonator. This is readily obtained for an exponentially increasing wave packet, as calculated both classically [22,38,39] and quantum mechanically [18,19], since the reflected and re-emitted signals increase in time together with opposite phase. For perfect destructive interference during the entire pulse, one must match the frequencies and set the drive amplitude time constant τ to $2/\kappa$ for a coupling leakage rate κ . Under these conditions, the absorption efficiency equals $1 - e^{-\kappa T}$ for a pulse of duration T (see the Supplemental Material [39]). The absorption efficiencies reach 99.4% for $\kappa T \geq 5.3$ and approach unity as $T \rightarrow \infty$. Using this idea, other protocols also permit perfect cancellation by temporally varying both the wave packet and κ [22].

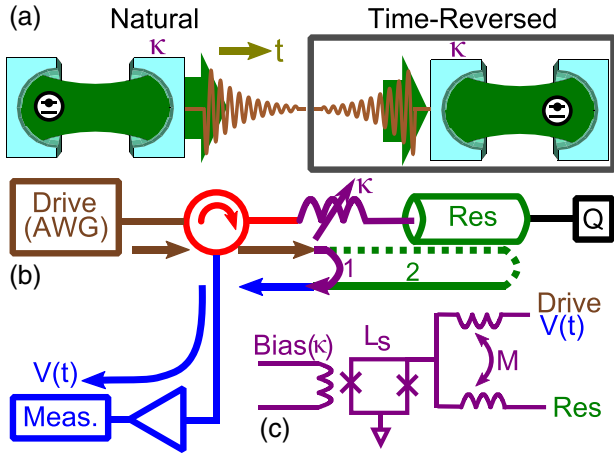


FIG. 1 (color online). Experimental design. (a) Natural decay of a photon state from a cavity, showing exponential decay with energy leakage rate κ . A time-reversed photon wave packet is thus absorbed by a cavity with 100% efficiency, as verified here (box). (b) Experimental setup showing shaped microwave pulse (drive) sent to the cavity (resonator) through a coupler (κ). An on/off tunable coupler allows separation of the capture, storage, and release processes, as well as calibration. An off-chip circulator separates the drive (brown arrows) coherent-state pulse generated by an arbitrary waveform generator (AWG) from the output $V(t)$ (blue arrows), measured with an amplifier and comprised of reflected (purple arrow, 1) and re-emitted (solid green, 2) signals that interfere destructively. The resonator is capacitively coupled to a superconducting phase qubit (Q) for calibration. (c) Schematic of tunable coupler. Coupler consists of two interwoven inductors with negative mutual inductance M and a SQUID with inductance L_s tuned by coupler bias line to vary κ .

Imperfect destructive interference between the reflected and re-emitted waves results in lower absorption efficiencies. The maximal absorption efficiency is only 81.45% [39] for a drive pulse with a rectangular or exponentially decreasing amplitude because initially the reflected signal has greater amplitude than the re-emitted signal, while at long times re-emission dominates. Reflections also do not cancel out re-emission if the resonator couples significantly to modes besides the drive; this results in a decreased efficiency as seen in Refs. [14,40,41].

To experimentally achieve the strong coupling necessary for complete destructive interference, we employ a tunable inductive coupler, shown in Figs. 1(b) and 1(c), through which we drive a 6.55 GHz superconducting coplanar waveguide resonator. This coupler has previously been used to emit shaped pulses [23]. The coupling is given by a mutual inductance modulated by a tunable superconducting quantum interference device (SQUID) inductance [23] and is calibrated using a superconducting phase qubit (see the Supplemental Material [39]). The resulting coupling can be tuned from negative couplings through zero (off) to $+1/(20 \text{ ns})$ in a few nanoseconds; as the drive pulse is similarly tuned in a few nanoseconds, the coupling can be

adjusted with the drive pulse to ensure reflection cancellation. We choose a coupling $\kappa = +1/(50 \text{ ns})$ for resonator driving and re-emission, which dominates over the intrinsic resonator loss $\kappa_i \approx 1/(3 \mu\text{s})$. By turning off the coupler, the absorbed energy is stored instead of immediately re-emitted.

We drive the resonator with a shaped pulse and measure the output voltage $V(t)$ versus time t to characterize the destructive interference. We generate a classical single-photon drive pulse using heterodyne mixing with an arbitrary waveform generator (see the Supplemental Material [39]) and concurrently set the coupling to $\kappa = +1/(50 \text{ ns})$ to capture the drive energy. Upon stopping the drive, we idle the coupler at $\kappa_{\text{off}} \approx 0$ [$|\kappa_{\text{off}}| \lesssim 1/(30 \mu\text{s})$] for 30 ns and then reset the coupling to κ to release the energy [see pulse sequence in Fig. 2]. During the entire sequence, we measure the complex $V(t)$ using two-channel heterodyne detection near the resonator frequency [39], averaging over 3×10^6 repetitions.

When the reflection and re-emission interfere destructively, $V(t)$ is comparable to the noise prior to the drive. This occurs only around 50 ns for an exponentially decreasing drive pulse [arrow in Fig. 2(a)]; elsewhere, either reflection [(1) in the middle panel] or re-emission [(2) in the middle panel] dominate. In contrast, the destructive interference lasts the entire drive for a properly shaped exponentially increasing pulse [Fig. 2(b)], implying high absorption efficiency.

We quantify this interference by the energy absorption efficiency. The energy measured through time t equals $E(t) = \int_0^t [|V(t')|^2 - N] dt' / 2R$ for $R = 50 \Omega$ and average noise power N [see bottom panel, Fig. 2]. The absorbed energy E_{abs} is the difference between the total drive energy $E(\infty)$ and the near-constant energy $E(\text{idle})$ at the idle. The absorption efficiency $E_{\text{abs}}/E(\infty)$ equals $(99.41 \pm 0.06)\%$ for the exponentially increasing drive but $(61.0 \pm 0.3)\%$ for the natural exponentially decreasing drive. This high absorption efficiency is independent of both the number of repetitions over which $V(t)$ is averaged and $E(\infty)$ for $E_{\text{abs}} = (0.5 \rightarrow 50)$ photons (see the Supplemental Material [39]). Note that we calibrate the energy scale by using the qubit to measure E_{abs} [39].

To achieve this high 99.4% absorption efficiency, we tune the pulse length T , exponential time constant τ , drive frequency f_d , and the timing of closing the coupler (see Fig. 3). For $\tau = 2/\kappa$, longer pulse lengths correspond to higher absorption efficiencies, reaching 99.4% for $T \geq 6/\kappa$ [Fig. 3(a)]. If τ is varied at $T = 20/\kappa$ [Fig. 3(b)], the absorption efficiency reaches the maximal 99.4% within 10% of $\tau = (2/\kappa)$ but falls to 90% for $\tau/(2/\kappa) = 2, 1/2$. In both cases, the efficiency falls off as expected.

We also tune the drive frequency f_d about the resonator frequency f_r , for a $T = 8/\kappa, \tau = 2/\kappa$ exponentially increasing drive pulse [Fig. 3(c)]. The absorption efficiency is maximized for $f_d = f_r$ and is at least 90% within $\pm 1 \text{ MHz}$

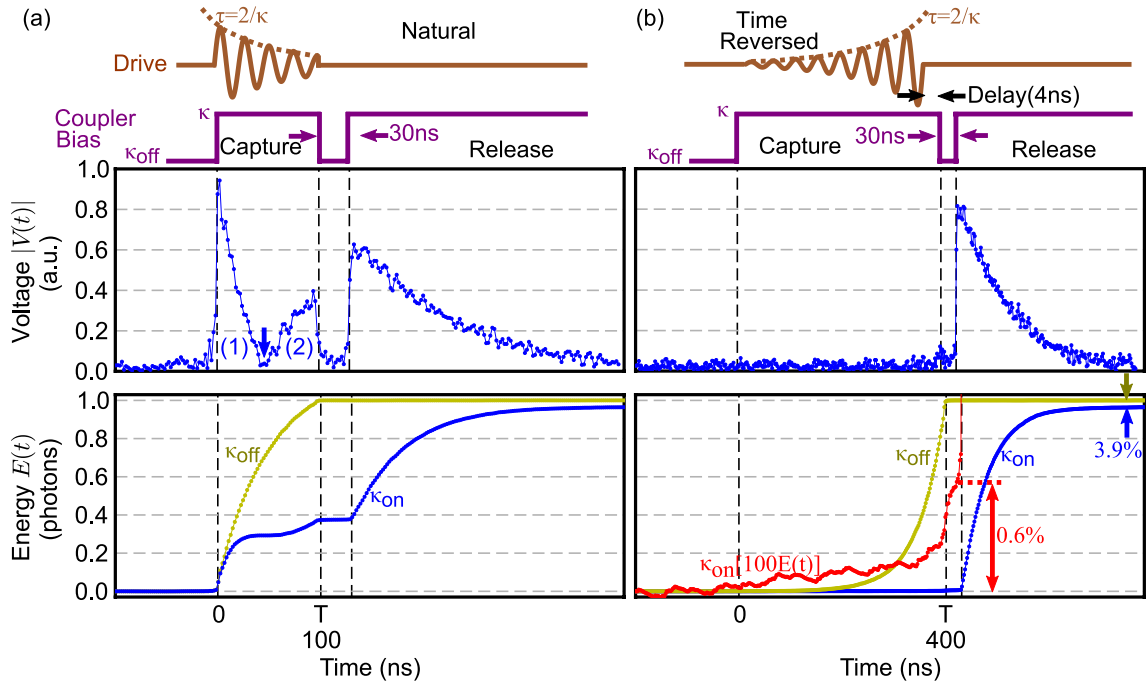


FIG. 2 (color online). Measurement protocol and data. Top: pulse sequence starts by driving the resonator with the coupler on using (a) a natural exponentially decreasing or (b) time-reversed exponentially increasing microwave pulse. Following the drive pulse, we close the coupler for 30 ns and reopen it to release the resonator energy. The packets have an energy of one photon and an amplitude time constant $\tau = 2/\kappa = 100$ ns and are truncated after length $T = 100$ ns (natural) or 400 ns (time reversed). Middle: measured output voltage versus time. The complex voltages $V(t)$ are averaged over 3×10^6 runs. For the natural wave packet (a), we see an initial reflection (1) and then resonator re-emission (2) in the capture period, followed by the release of the stored energy. At the arrow, the reflection and re-emission signals cancel and the phase of $V(t)$ changes by π (see the Supplemental Material [39]). For the time-reversed packet (b), little microwave power is observed in the capture period, indicating high efficiency. Bottom: blue (κ_{on}) curves show measured energy $E(t)$, obtained by subtracting the average noise power from $|V(t)|^2$ and then integrating over time. Gold (κ_{off}) curves show the calibration signal of the reflected incoming packet, with the coupler always off. In panel (b) the red ($\kappa_{\text{on}}[100E(t)]$) curve is a 100 \times expanded scale, showing small reflected energy. The energy at the end of the capture period, normalized to the total energy at long times, gives the absorption error; we find absorption efficiencies of $(61.0 \pm 0.3)\%$ for the natural case and $(99.41 \pm 0.06)\%$ for the time-reversed case. Normalizing to the total incident energy (gold, κ_{off}), we measure a $[95.5 \pm 1.2]\%$ ($[97.4 \pm 0.6]\%$) storage (receiver) efficiency for the time-reversed wave packet.

of f_r . According to theory, achieving an appreciable absorption efficiency requires $f_d = f_r$ to within a linewidth $\kappa/2\pi = 3$ MHz [39].

To achieve the 99.4% absorption efficiency, we must delay closing the coupler relative to turning off the drive even after calibrating the coupler-resonator timing (see Supplemental Material [39]). The absorption efficiency is reduced by 10% when the delay differs by 3.5 ns from the optimal 4.5 ns [Fig. 3(d)]. The efficiency decreases since the entire drive is reflected if the coupler is closed too early and some of the captured energy is re-emitted if the coupler is closed too late. The scaling is linear for delays longer (shorter) than the optimum due to the sharpness of turning off the drive (closing the coupler). We observe experimental deviations from the linear slope for shorter delays, so our coupler pulse shaping is nonideal, possibly explaining why the offset is required.

To demonstrate the necessity of appropriate pulse shaping, we measured the absorption efficiencies for rectangular

[Fig. 4(a)], truncated exponentially decreasing [Fig. 4(c)], and exponentially increasing drive pulses [Fig. 4(e)] versus pulse length T and exponential time constant τ . All three pulse shapes have similar shapes and hence absorption efficiencies for $\tau > 10T$. For rectangular pulses, the maximal absorption efficiency is $\sim 79\%$ compared to the predicted 81.5%; this limit also provides the maximal absorption efficiencies for exponentially decreasing pulses. The efficiency is reduced because no initial excitation exists for which re-emission can cancel the initial reflections [see (1) in the middle panel of Fig. 2(a)]. In addition, these experimental efficiencies agree with the theoretical efficiencies [Figs. 4(a), 4(b), and 4(d)] to within $\sim 4\%$, with possible error sources including calibration and pulse shaping errors. Both theory and experiment show that the only pulses with 99.4% absorption efficiencies are exponentially increasing pulses with $\tau = 2/\kappa$ and $T \geq 6/\kappa$.

However, the absorption efficiencies neglect intrinsic resonator losses κ_i . To measure this effect, we drive the

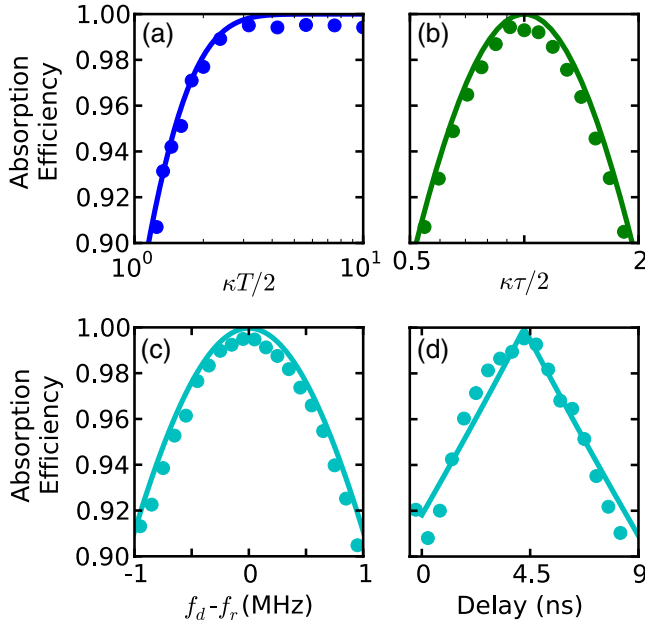


FIG. 3 (color online). Tuning up 99.4% absorption efficiency. As shown in the pulse sequence of Fig. 2(a), the four parameters which must be tuned up precisely are (a) the pulse length T , (b) time constant τ , (c) the detuning of the drive frequency f_d relative to the resonator frequency f_r , and (d) the time delay of closing the coupler after stopping the resonator drive. The absorption efficiencies are maximized for an exponentially increasing pulse by $\tau = 2/\kappa$, $T \geq 5.3/\kappa$, $f_d = f_r$, and a 4.5 ns delay. In all cases the experimental absorption efficiencies (points) fall off as expected theoretically (lines: see the Supplemental Material [39]). Data are for single-photon drives with $\kappa = 1/(50 \text{ ns})$ and (a) $\tau = 2/\kappa$, (b) $T = 20/\kappa$, and (c)–(d) $\tau = 2/\kappa$ and $T = 8/\kappa$, as per the colored slices in Fig. 4(e). Uncertainties are $\leq 0.14\%$ [39].

resonator with the coupler off (κ_{off}) and measure the total reflected energy E_{off} . We compare this to the total measured energy E_{on} when we drive the resonator at κ . The fraction of energy not lost is $E_{\text{on}}/E_{\text{off}} = 96.1\%$ [Fig. 2(b), bottom panel]. The storage efficiency for the entire process, $(95.5 \pm 1.2)\%$, is $E_{\text{on}}/E_{\text{off}}$ times the absorption efficiency. However, this efficiency includes losses from κ_i during both the capture and release phases. During just the drive, we keep approximately $\sqrt{E_{\text{on}}/E_{\text{off}}} = 98.1\%$ of the energy assuming near-perfect absorption [14]. This fraction times the absorption efficiency is the receiver efficiency, which equals $(97.4 \pm 0.6)\%$ for the optimal pulse.

A primary limitation on the receiver efficiency is the resonator coherence. We expect to keep $\kappa/(\kappa + \kappa_i) = 98.4\%$ (see the Supplemental Material [39]) of the energy, close to the measured 98.1%. Although this is limited by $1/\kappa_i = 3 \mu\text{s}$, we have since fabricated resonators with coherence times $1/\kappa_i = 45 \mu\text{s}$ [42]. With such resonators, the 300 ns minimum high-efficiency pulse length is negligible compared to $1/\kappa_i$ and the receiver efficiency should reach $> 99\%$. Additional error sources, which also

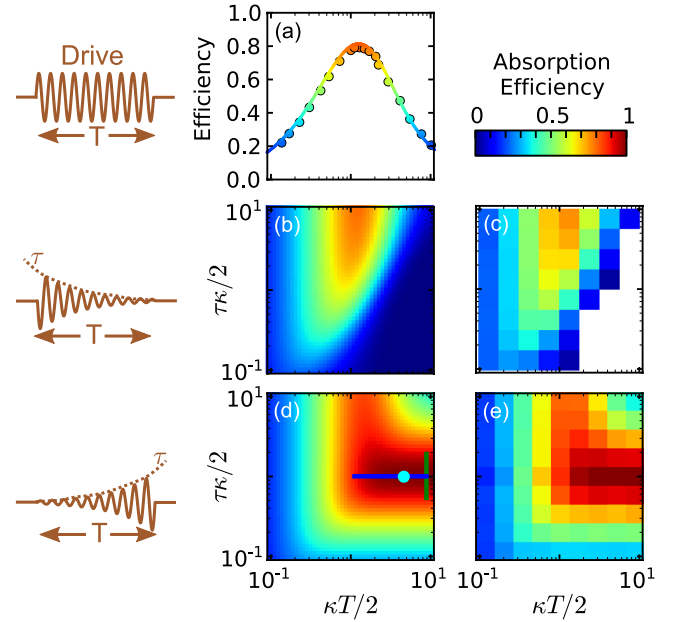


FIG. 4 (color online). Absorption efficiencies versus pulse shape. Theoretical and experimental absorption efficiencies (color, grayscale) are plotted versus pulse length T and exponential time constant τ . Experimental data are for single-photon drives with couplings (a), (c) $\kappa = 1/(40 \text{ ns})$, and (e) $\kappa = 1/(50 \text{ ns})$ and have uncertainties $\leq 0.4\%$ (see the Supplemental Material [39]). Theory has no fit parameters. (a) Rectangular drive pulse (theory and experiment). Absorption efficiencies are maximized at 79% (81.5% theory) for $T \approx 2.5/\kappa$. (b)–(c) For a truncated exponentially decreasing drive pulse, theoretical (b) and experimental (c) absorption efficiencies are maximized as $\tau \rightarrow \infty$, the rectangular pulse limit, with efficiencies similar to (a). (d)–(e) For a truncated exponentially increasing drive pulse, theoretical (d) and experimental (e) absorption efficiencies are maximized for $\tau = 2/\kappa$ and $T \geq 6/\kappa$ at 99.4% (100% theory).

limit the minimum pulse length (see the Supplemental Material [39]), likely include pulse-calibration imperfections and the measurement system resolution. In addition, thermal noise can swamp microwave photon signals passing through room-temperature cables in a long-distance quantum network. Such thermal effects do not affect the efficiency, however, for quantum networks connecting numerous chips in a single cryostat, which are key for building large-scale or hybrid quantum computers.

Our approach is a receiver building block for the complete state transfer in a quantum network. The shaped release of Fock states, which can be generated by various qubit types and swapped to a superconducting resonator [10–14], has been demonstrated and is phase coherent [23]. Theoretically, such states, shaped as described here, can be completely absorbed by qubits [18,19]; this process is equivalent to shaped single-photon Fock states being perfectly absorbed by resonators.

In conclusion, we have demonstrated coherent-state energy absorption with efficiencies above the fault-tolerant

threshold for deterministic quantum communication when driving a superconducting coplanar waveguide resonator with exponentially increasing pulses. With this time-reversed drive, the reflected and re-emitted signals are effectively canceled, resulting in energy absorption efficiencies of 99.4% (97.4%) without (with) including decoherence. These efficiencies enable inter-chip deterministic interconnects for complex large-scale or hybrid quantum computers.

Devices were made at the UC Santa Barbara Nanofabrication Facility, part of the NSF-funded National Nanotechnology Infrastructure Network. This research was funded by the Office of the Director of National Intelligence (ODNI), Intelligence Advanced Research Projects Activity (IARPA), through Army Research Office Grant No. W911NF-10-1-0334. All statements of fact, opinion, or conclusions contained herein are those of the authors and should not be construed as representing the official views or policies of IARPA, the ODNI, or the U.S. Government.

*martinis@physics.ucsb.edu

- [1] G. Kirchmair, B. Vlastakis, Z. Leghtas, S. E. Nigg, H. Paik, E. Ginossar, M. Mirrahimi, L. Frunzio, S. M. Girvin, and R. J. Schoelkopf, *Nature (London)* **495**, 205 (2013).
- [2] H. Wang *et al.*, *Phys. Rev. Lett.* **106**, 060401 (2011).
- [3] A. F. van Loo, A. Fedorov, K. Lalumière, B. C. Sanders, A. Blais, and A. Wallraff, *Science* **342**, 1494 (2013).
- [4] I.-C. Hoi, C. M. Wilson, G. Johansson, J. Lindkvist, B. Peropadre, T. Palomaki, and P. Delsing, *New J. Phys.* **15**, 025011 (2013).
- [5] A. Miranowicz, M. Paprzycka, Y. X. Liu, J. Bajer, and F. Nori, *Phys. Rev. A* **87**, 023809 (2013).
- [6] B. Peropadre, G. Romero, G. Johansson, C. M. Wilson, E. Solano, and J. J. García-Ripoll, *Phys. Rev. A* **84**, 063834 (2011).
- [7] A. Reiserer, S. Ritter, and G. Rempe, *Science* **342**, 1349 (2013).
- [8] Z.-L. Xiang, S. Ashhab, J. Q. You, and F. Nori, *Rev. Mod. Phys.* **85**, 623 (2013).
- [9] M. Wallquist, K. Hammerer, P. Rabl, M. Lukin, and P. Zoller, *Phys. Scr.* **T137**, 014001 (2009).
- [10] J. Majer *et al.*, *Nature (London)* **449**, 443 (2007).
- [11] S. D. Hogan, J. A. Agner, F. Merkt, T. Thiele, S. Filipp, and A. Wallraff, *Phys. Rev. Lett.* **108**, 063004 (2012).
- [12] D. I. Schuster *et al.*, *Phys. Rev. Lett.* **105**, 140501 (2010).
- [13] Y. Kubo *et al.*, *Phys. Rev. Lett.* **105**, 140502 (2010).
- [14] T. A. Palomaki, J. W. Harlow, J. D. Teufel, R. W. Simmonds, and K. W. Lehnert, *Nature (London)* **495**, 210 (2013).
- [15] S. Ritter, C. Nölleke, C. Hahn, A. Reiserer, A. Neuzner, M. Uphoff, M. Mücke, E. Figueroa, J. Bochmann, and G. Rempe, *Nature (London)* **484**, 195 (2012).
- [16] L. Steffen, Y. Salathe, M. Oppliger, P. Kurpiers, M. Baur, C. Lang, C. Eichler, G. Puebla-Hellmann, A. Fedorov, and A. Wallraff, *Nature (London)* **500**, 319 (2013).
- [17] H. J. Kimble, *Nature (London)* **453**, 1023 (2008).
- [18] M. Stobińska, G. Alber, and G. Leuchs, *Europhys. Lett.* **86**, 14007 (2009).
- [19] Y. Wang, J. Minář, L. Sheridan, and V. Scarani, *Phys. Rev. A* **83**, 063842 (2011).
- [20] J. I. Cirac, P. Zoller, H. J. Kimble, and H. Mabuchi, *Phys. Rev. Lett.* **78**, 3221 (1997).
- [21] K. Jahne, B. Yurke, and U. Gavish, *Phys. Rev. A* **75**, 010301 (R) (2007).
- [22] A. N. Korotkov, *Phys. Rev. B* **84**, 014510 (2011).
- [23] Y. Yin *et al.*, *Phys. Rev. Lett.* **110**, 107001 (2013).
- [24] S. J. Srinivasan, N. M. Sundaresan, D. Sadri, Y. Liu, J. M. Gambetta, T. Yu, S. M. Girvin, and A. A. Houck, *Phys. Rev. A* **89**, 033857 (2014).
- [25] M. Pechal, C. Eichler, S. Zeytinoglu, S. Berger, A. Wallraff, and S. Filipp, *arXiv:1308.4094 [Phys. Rev. X (to be published)]*.
- [26] M. Bader, S. Heugel, A. L. Chekhov, M. Sondermann, and G. Leuchs, *New J. Phys.* **15**, 123008 (2013).
- [27] A. G. Fowler, D. S. Wang, C. D. Hill, T. D. Ladd, R. Van Meter, and L. C. L. Hollenberg, *Phys. Rev. Lett.* **104**, 180503 (2010).
- [28] A. G. Fowler, M. Mariani, J. M. Martinis, and A. N. Cleland, *Phys. Rev. A* **86**, 032324 (2012).
- [29] D. L. Moehring, P. Maunz, S. Olmschenk, K. C. Younge, D. N. Matsukevich, L.-M. Duan, and C. Monroe, *Nature (London)* **449**, 68 (2007).
- [30] J. Hofmann, M. Krug, N. Ortegel, L. Gérard, M. Weber, W. Rosenfeld, and H. Weinfurter, *Science* **337**, 72 (2012).
- [31] C. Kurz, M. Schug, P. Eich, J. Huwer, P. Müller, and J. Eschner, *arXiv:1312.5995*.
- [32] J. M. Chow *et al.*, *Phys. Rev. Lett.* **109**, 060501 (2012).
- [33] J. E. Johnson, C. Macklin, D. H. Slichter, R. Vijay, E. B. Weingarten, J. Clarke, and I. Siddiqi, *Phys. Rev. Lett.* **109**, 050506 (2012).
- [34] K. Geerlings, Z. Leghtas, I. M. Pop, S. Shankar, L. Frunzio, R. J. Schoelkopf, M. Mirrahimi, and M. H. Devoret, *Phys. Rev. Lett.* **110**, 120501 (2013).
- [35] R. Barends *et al.*, *Nature (London)* **508**, 500 (2014).
- [36] E. Jeffrey *et al.*, *Phys. Rev. Lett.* **112**, 190504 (2014).
- [37] J. D. Jackson, *Classical Electrodynamics* (Wiley, New York, 1999).
- [38] S. Heugel, A. S. Villar, M. Sondermann, U. Peschel, and G. Leuchs, *Laser Phys.* **20**, 100 (2010).
- [39] See Supplemental Material at <http://link.aps.org/supplemental/10.1103/PhysRevLett.112.210501> for derivations of theoretical absorption efficiencies, details of the experimental setup (including calibrations, independence on drive power, and effect of averaging), and derivation of the error analysis.
- [40] S. A. Aljunid, G. Maslennikov, Y. Wang, H. L. Dao, V. Scarani, and C. Kurtsiefer, *Phys. Rev. Lett.* **111**, 103001 (2013).
- [41] S. Zhang, C. Liu, S. Zhou, C.-S. Chuu, M. M. T. Loy, and S. Du, *Phys. Rev. Lett.* **109**, 263601 (2012).
- [42] A. Megrant *et al.*, *Appl. Phys. Lett.* **100**, 113510 (2012).